Low cost, high performance spray pyrolysis grown amorphous Zinc Tin Oxide: The challenge of a complex growth process

Ainur Zhussupbekova,*,† David Caffrey,† Kuanysh Zhussupbekov,† Christopher M. Smith,† Igor V. Shvets,† and Karsten Fleischer‡

†*School of Physics and Centre for Research on Adaptive Nanostructures and Nanodevices (CRANN), Trinity College Dublin, Dublin 2, Ireland*

‡*School of Physics, Dublin City University, Dublin 9, Ireland*

E-mail: zhussupa@tcd.ie

Abstract

Transparent conductive oxides (TCOs) are important materials for a wide range of optoelectronic devices. Amorphous zinc-tin oxide (a-ZTO) is a TCO and one of the best non toxic, low-cost replacement for more expensive amorphous indium- gallium-zinc oxide. Here, we employ spray pyrolysis, an inexpensive and versatile chemical vapour deposition based technique, to synthesise a-ZTO with an as-deposited conductivity of ≈300 S/cm – the highest value hitherto among the reported solution processed films. Compositional analysis via X-ray photoelectron spectroscopy reveals a non-stoichimoetric transfer of Zn and Sn from the dissolved precursors into the film, with best electrical properties achieved at a film composition of x_{film}=0.38±0.04 ($(ZnO)_x(SnO_2)_{1-x}$ ($0<x<1$)). The morphology of these films is compared to films synthesised by physical vapour deposition, and a strong correlation between morphology and electrical properties is revealed. A granular nature of the SP grown films, which seems

like a drawback at a first glance, brings a prospect of using a-ZTO in ink-jet printed films from a nanoparticle suspension for the room temperature deposition. Brief post-anneal cycles in N_2 gas improve the conductivity of the films by means of grain boundary passivation.

Keywords

Transparent Conducting Oxide, TCO, amorphous oxide semiconductor, Zinc Tin Oxide, ZTO, Spray Pyrolysis, X-ray photoelectron spectroscopy, XPS

1 Introduction

Amorphous indium-gallium-zinc oxide (a-IGZO) has taken a dominant place in the field of amorphous Transparent Conducting Oxides (a-TCOs) due to its impressive conductivity, controllable carrier concentration, ease of manufacturing, and high mobility.[1,2] Nevertheless, there are some sustainability concerns raised by the indium content of the material related to the toxicity,[3] inflexibility of supply and increasing costs of its constituent elements.[4] This creates a demand for a new generation of sustainable, low cost materials[5] with improved mechanical properties[6] and thermal stability due to their amorphous nature[7] for the development of the electronics industry.[8] Amorphous zinc-tin oxide (a-ZTO) occupies this niche,[9,10] being entirely composed of Earth abundant elements and possessing a high direct optical bandgap of 3.3-3.9 eV,[11] high optical transparency and good electrical properties, with conductivities of up to 445 S/cm reported.[12–14] a-ZTO possess the same overlapping *s*-orbital dominated dispersed conduction band structure as a-IGZO[15] leading to a high mobility and conductivity, that is maintained even in absence of a crystal structure. a-ZTO has already been utilised in laboratory scale thin film transistors,[11,16–18] photovolatic cells,[19] gas sensing,[20] transport channels in metal-semiconductor-field-effect-transistors[21,22] and organic light-emitting diodes (OLEDs).[13,23]

a-ZTO has been grown by a variety of physical vapour deposition (PVD) methods including magnetron sputtering,[11,13,24] pulsed laser deposition[25] and some chemical methods.[21,26–29] The

most common chemical method is spin-coating, however this can be associated with an unwanted increased degree of porosity.[30] Synthesis of these films via spray pyrolysis (SP) technique, where decomposition of precursors occurs as a result of spraying a solution over a heated substrate, is highly desirable due to the method's low-cost and versatility. In spite of this, there are practical challenges which hinder wider application of SP to a-ZTO. High quality a-ZTO is a non trivial material to synthesise with a wide range of different defects[12,31] and local structures[32–35] which easily form under nominally similar deposition conditions. While this impacts all growth techniques, the effect is exacerbated for SP by the complexity of the physics of the precursor delivery and the chemical synthesis steps. As in-lab construction and customisation is the norm for the technique, this additional complexity is in turn accentuated by the absence of standardisation across SP deposition systems, with liquid delivery, nebulisers, substrate heating, and atmosphere management systems all varying. As a result, an understanding of the role of system parameters in determining film properties is required to allow transference of results between laboratories and eventually to large scale tools.

Here we report on the synthesis of high performance a-ZTO via a single step deposition SP technique. We obtain conductivities of 330 S/cm, highest reported CVD grown up to date, under optimised growth and brief post-growth treatment. Fabrication simplicity, cost-effectiveness, low optical absorption and roughness highlight the potential applicability of the proposed method for efficient light emission and minimum current leakage through the organic active layers in OLEDs.[13] We identify film morphology as being the primary limiting factor in electrical performance and link this to inherent factors in our deposition set up. In doing so, we present a roadmap by which the performance of SP grown ZTO can be further improved to match and even surpass the best PVD grown films[12,13] without costly, energy-consuming vacuum conditions and high voltages.

2 Experimental details

Full details of the chamber geometry, nozzle type, etc. employed in this work are reported elsewhere.[36] Key to the following discussion is that we only employ a simple gas blast nebuliser (PNR, model 0331). All films were deposited on standard microscopy glass slides (Thermo Scientific, 2.5×5 cm, 1 mm thick). Precursors of Zinc chloride and Tin (II) 2-thylehexanoate were dissolved in methanol keeping the total molarity constant at 0.05 M. The concentration of Sn and Zn precursor was changed according to: c_{Zn}=x_{sol}·0.05 M and c_{Sn}=$(1-x_{sol})\cdot 0.05$ M, with x_{sol} varied from 0.2 to 0.8 in steps of 0.05. These specific precursors were selected for their high solubility in methanol, with no precipitation being observed and without need for any extensive stirring. The solution was sprayed at a rate of 1.7 ml/min using a mixture of compressed air and nitrogen with a gas flow of 17 l/min onto a heated substrate with a heater temperature of 450 °C. A gas composition of 95% nitrogen /5% oxygen was observed to give maximum performance of as grown films. The temperature readings from the heater surface during the growth were taken using a type K thermocouple (chromel vs. alumel) welded to the top of the hot plate. The heater temperature was PID controlled during spray conditions within ±10 °C. Due to the cooling effect of the gas flow, actual substrate surface temperatures is assumed to be lower.

Room temperature electrical properties were determined via Hall measurements using Van der Pauw methodology with silver wire contacts attached to the surface via silver adhesive. X-ray diffraction (XRD) was used to verify the amorphous nature of all deposited films (see Supplementary Information (SI) Figure S2). For films thinner than 120 nm X-ray reflection (XRR) was employed to confirm precise film thickness. As XRR requires a low surface roughness, its use here already indicates the high quality of the deposited films. Substantially thicker films (all in a range of 200 nm) were measured by spectroscopic ellipsometry (Sopra GESP 5) using three incidence angles around the Brewster angle (63°, 66°, 69°). Representative fits for the thickness determination by XRR and Ellipsometry are depicted in Figure 1(c, d). Morphology of the films was studied by scanning electron microscopy (SEM) on a Zeiss SEM Ultra microscope with 3-5 keV electron energies. Topography of the films was obtained by atomic force microscopy (AFM) (see SI Figure

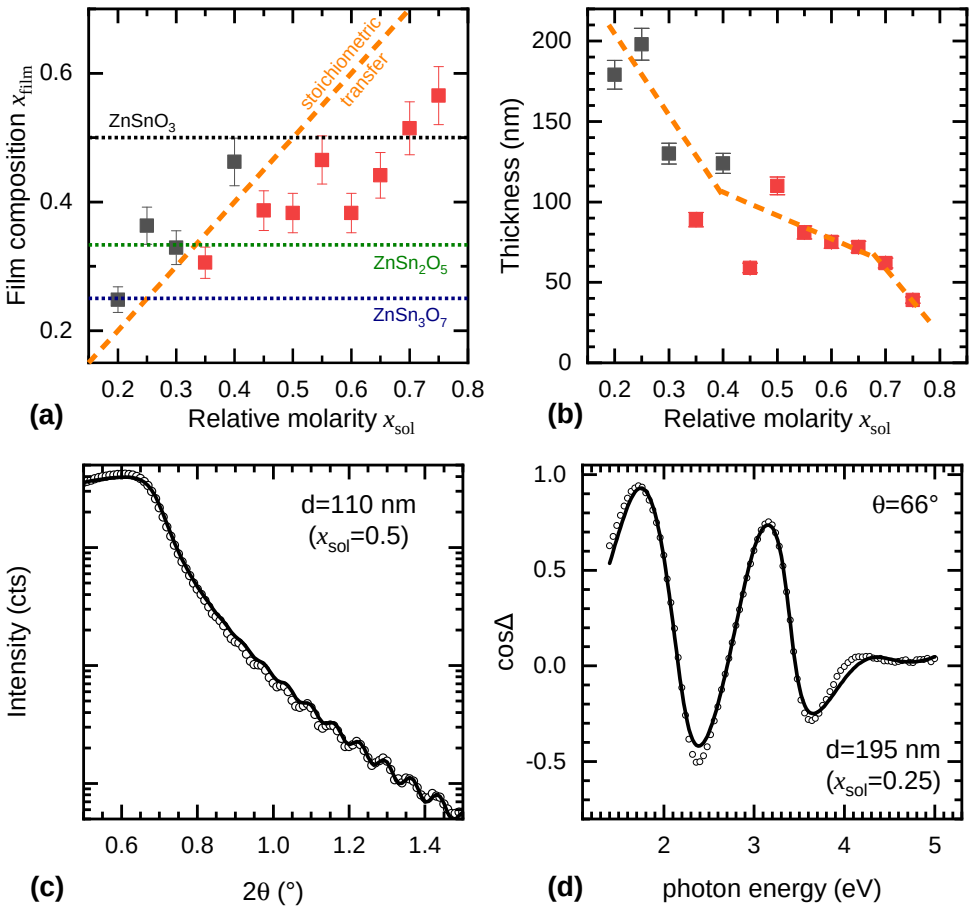

Figure 1: (a) Film composition as function of solution relative molarity. The orange dashed line indicates the case of stoichiometric transfer from solution. As a guide, compositions consistent with some calculated crystalline ZTO phases have been included; (b) Thickness vs. solution relative molarity; for thicker samples shaded in grey, thickness was obtained via ellipsometry (c) Representative raw XRR data and corresponding fit (d) Representative raw ellipsometry data and corresponding fit.

S4). Optical properties were measured via UV-Visible spectrophotometry (Perkin Elmer S650). Thermal postgrowth treatments were carried out in full nitrogen atmosphere in a separate Bell-jar chamber. The thin-film resistivity was measured in situ by four-point probe measurements using spring loaded gold contacts in linear configuration with a Keithley 2400 source meter. The film resistivity was recorded during a 50 °C → 290 °C → 50 °C annealing cycle with a total process time of 15 min.[37]

To evaluate the stoichiometry of the films, X-ray photoelectron spectroscopy (XPS) was used (Omicron Multiprobe XPS; monochromized Al Kα source (XM 1000, 1486.7eV); EA125 U5 analyser). Prior to measurement all films were sonicated in acetone and isopropanol with further Ar ion etching (750 V; sputter current ≈6 µA; pressure 1.5×10^{-3}Pa; 10 min). This ensures the removal of unreacted precursors on the surface. Total intensity of the Zn 2p and Sn 3p were used in determining Zn/Sn ratio using CasaXPS (corrected for cross section and electron escape depth, see SI Figure S1). As the sputter cleaning cycle can potentially induce chemical shifts via surface band bending and/or preferential removal of oxygen, we do not attempt to deduce oxygen content and oxidation state of Sn, assuming thermodynamically more stable Zn^{+2} and Sn^{+4} to be prevalent. We report the film composition in terms of the x value from the expression $(ZnO)_x(SnO_2)_{1-x}$ $(0<x<1)$[11]. In this work we will refer to the composition of the film using x_{film}, while the precursor solution cation ratio will be notated as x_{sol}. A complete stoichiometric transfer from solution to film would result in x_{sol}=x_{film} (orange dashed line in Figure 1(a)).

3 Results and discussion

Figure 1(a) compares the solution concentration with the Zn content found in the film. Stoichiometric transfer from solution to film is only observed at a high Sn content ($x_{\text{sol}}<0.4$). Once the Zn content exceeds $x_{\text{sol}}>0.4$, the film composition remains relatively constant. For $x_{\text{sol}}>0.65$ the Zn content increases again. This is consistent with a kinetic limitation of film growth by the Sn molarity. The surplus Zn within the solution is not incorporated, consequently a reduction of the growth

rate is seen (Figure 1(b)). This behaviour complicates the growth due to the high dependence of the defect chemistry of a-ZTO on its Sn stoichiometry, with previous reports demonstrating that the primary donor defect in a-ZTO result from under-coordinated metal Sn ions.[31] In the range ($0.4<x_{\mathrm{sol}}<0.65$), changing the cation ratio in solution does not significantly alter the composition, but will alter the growth rate and hence defect formation in the films. As a consequence, films with the same x_{film} exhibit different properties due to their differing x_{sol} in their respective growth run.

The conductivity, carrier mobility, and carrier concentration of the films are displayed in Figure 2. Electrical performance of the films vary dramatically and, if shown in terms of film composition (x_{film}), a large scatter of the data is seen. Despite this, a clear general trend in conductivity, dictated by carrier concentration, can be observed. It is important to note that at optimised growth conditions, *as-deposited* films can already demonstrate degenerate conductivity of 304 S/cm and carrier concentration 2×10^{20} cm^{-3}. This electrical performance is already comparable with samples grown via PVD[13,24] and is only exceeded by reports utilising defect passivation by post-growth treatments.[12] This highlights the high potential of films grown via SP. To further increase the performance of these films we need to identify both the limiting factor in these films performance and, more importantly, the cause for the apparent scatter within films of otherwise similar stoichiometry.

The carrier concentration was found to vary monotonically (see Figure 2c), with little scattering and is comparable, if not in excess, of values obtained by magnetron sputtering in our facilities[24] and elsewhere.[11,13] Conductivity variations were instead driven by large variations in the mobility. Best samples show high mobilities with a maxima of 9-10 cm^2/Vs being observed for a wide range of film compositions, but this is a noticeable reduction from literature best values of >16 cm^2/Vs,[13,32,35] which are achieved without special treatments.

Limited carrier mobility can occur due to defect scattering or macroscopic grain boundary (GB) scattering. We refer to it as a GB despite the amorphous nature of the films. Previous studies have demonstrated that there is an inverse relationship between the number of donor defects in a-ZTO and its mobility at high levels of carriers.[12] However, in these SP grown films a similar

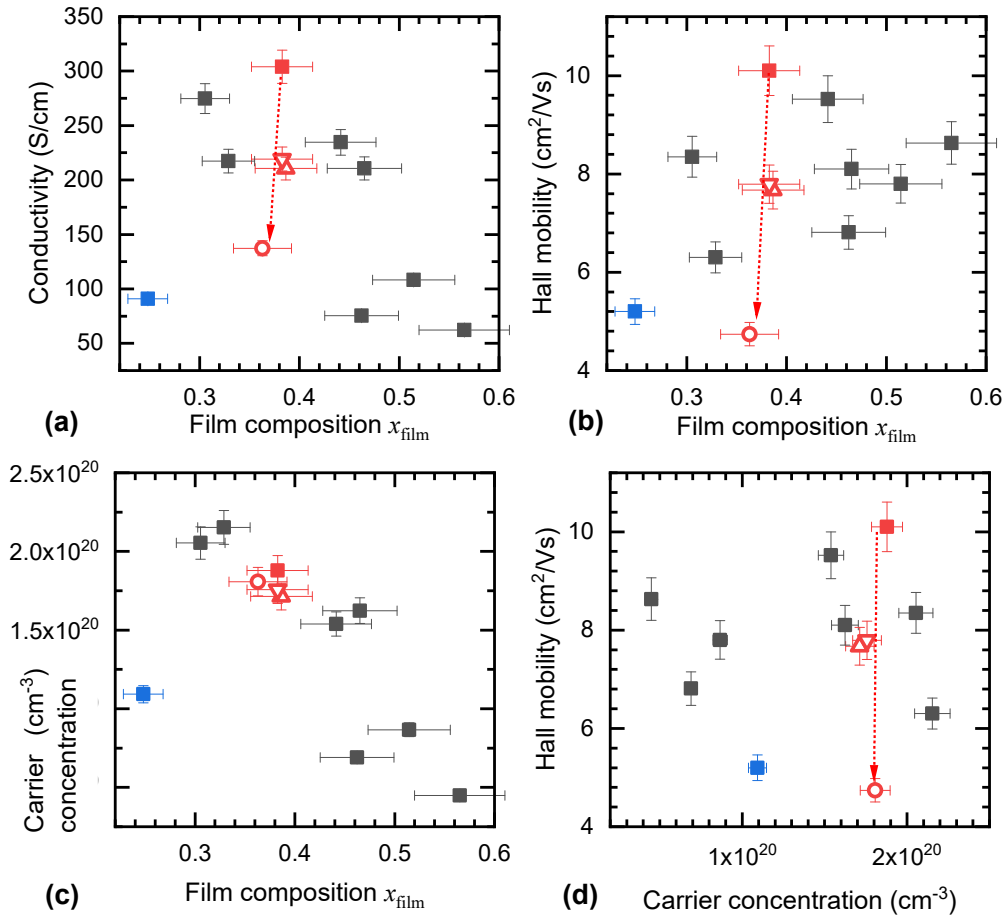

Figure 2: Dependency of electrical properties on film stoichiometry x_{film}: (a) conductivity, (b) Hall mobility, (c) carrier concentration. (d) mobility as a function of a carrier concentration. Only the carrier concentration is strongly dependent on the overall film stoichiometry. A subset of samples with similar x_{film} is highlighted in red. While they posses similar carrier concentration their mobilities differ due to morphological differences in the films. The Sn-rich sample for x_{film}=0.25 (blue) does not follow the general trend due to an additional de-phasing of the film (see SI Figure S2).

mobility is obtained independently of the carrier concentration (see Figure 2d). In addition, it can be observed that the maximum mobility occurs at high carrier concentrations, opposite the expectation for a mobility limited by ionised impurity scattering. In addition, in most reported studies of ZTO mobility is enhanced at Zn rich compositions, an effect not observed here.[13,24] We therefore suggest that for these SP grown samples, the mobility is hindered by a granular nature of the films themselves. It should be noted that a granular structure does not imply a crystalline material. At a simple level, SP deposition combines two processes: 1) individual nucleation of dried up seed material from liquid phase growth within droplets and 2) a CVD type of growth which increases the size of those nucleates within the atmosphere above the growing film and after their adhesion onto the film.[38] Therefore, SP films frequently demonstrate granular features independent of the crystallinity. Grazing incidence XRD measurements have shown no discernible crystalline structure in most cases (see SI Figure S2). Only the most Sn rich sample (x_{film}=0.25), which also has anomalous electrical properties, exhibits a partial de-phasing of the films into SnO_2 and a-ZTO in these conditions.

Figure 3 shows SEM images of a-ZTO grown via spray (a, b, c, d) and via magnetron sputtering (e, f). A comparison of spray and magnetron grown films yield some immediate differences in morphology, with magnetron films being continuous smooth films with no discernable structure, while SP films demonstrate an observable granular structure. We attribute the overall lower mobility in spray grown films compared to magnetron ones to this granular structure, with the resulting GB scattering being the limiting factor. It is important to note that the occurrence of a granular structure is not necessarily a consequence of the SP method itself, but more likely arises from constraints introduced by the insufficient nebulisation of the solution in the utilised air-blast nozzle. An improvement in the quality of deposited films could therefore simply be achieved by the use of ultrasonic nebulisers known to produce smaller droplets and narrower droplet size distributions which will help to achieve more CVD like conditions and minimise the morphological damage and clustering of larger liquid droplets impacting the surface.

A comparison of data from SEM, XRR and AFM can be used to explain the observed mobil-

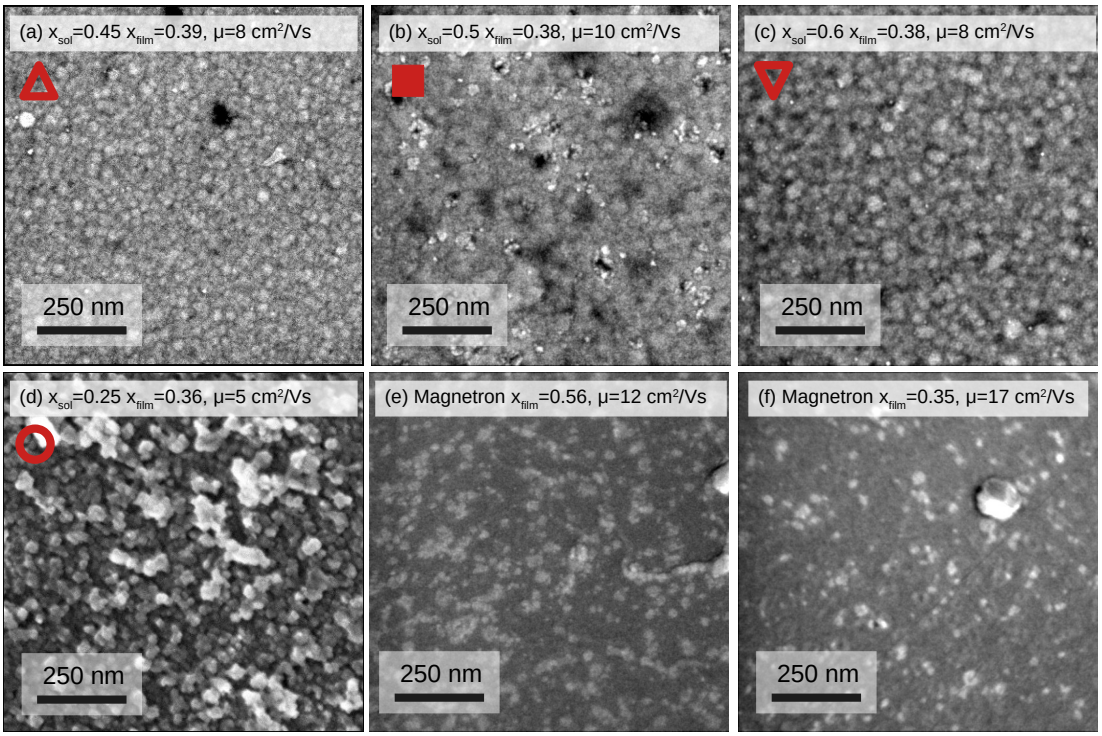

Figure 3: (a-d) SEM images of a-ZTO with similar composition $x_{\text{film}}\approx 0.38$, from SP growth runs with varying solution composition (b) has the highest conductivity of 304 S/cm and mobility value of 10 cm^2/Vs; (a, c) are samples with lower conductivity of 220 S/cm due to lower mobility of 8 cm^2/Vs. (d) is slightly more Sn rich and has an even lower mobility. (e-f) Magnetron sputtering grown a-ZTO with varying film composition for comparison.

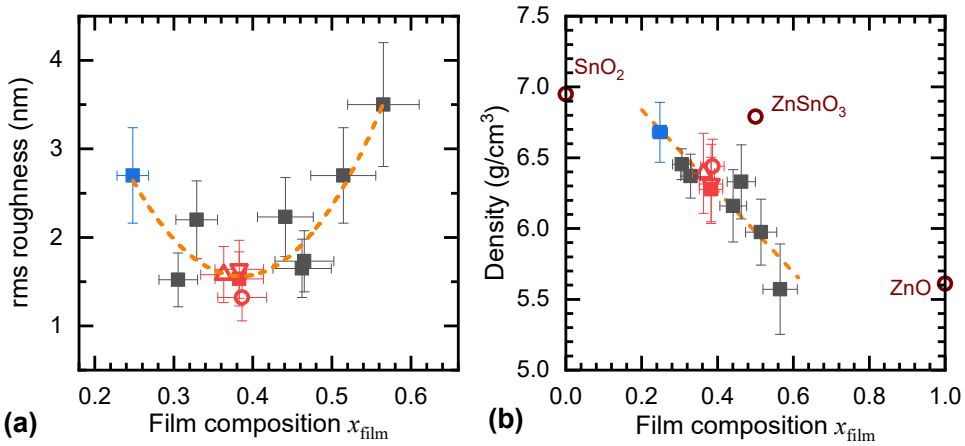

Figure 4: XRR analysis of (a) rms roughness and (b) density as function of measured sample stoichiometry. Displayed error bars are estimated by variation in fitting results using different roughness models, fitting software, and range limitations, to account with the systematic errors in XRR-analysis. Density of crystalline phases $ZnSnO_3$ (01-077-4192), ZnO (01-070-8070) and SnO_2 (01-071-53-24) phases have been taken from database and included for a comparison.

ity variations, most notably at $x_{film} \approx 0.38$. Figure 3 demonstrates that the surfaces of four spray deposited films composed of a mixture of differently shaped particles that are closely packed. No large macroscopic cracks and fissures are observed in these films, indicating that the issues do not originate from substrate heating or cooling induced damage due to thermal mismatches and consequent film delamination. The most noticeable difference is that the granular structure in samples with lower mobility is more pronounced and individual grains appear more separated. Thus the reduction in mobility is consistent with an increase in number of GBs or porosity in the film.

SEM images show the changes in morphology qualitatively but is supported by more quantitative measurements using XRR and AFM. Least-square fits of the XRR measurements, mainly used to determine the thickness, can also provide estimates for the root mean square (rms) roughness, as well as density of the films. Figure 4 shows that best films around $x_{film} \approx 0.38$ are smoothest, while the density of the films linearly depends on the Sn content. AFM measurements (see SI Figure S3 and S4) broadly confirm the general trend.

The granular structure of the film explains why SP grown samples show a lower mobility and little dependence on the Zn content itself. In a GB restricted mobility model, an improvement in transport in the material itself is not observed on the macroscopic transport once GB scattering is

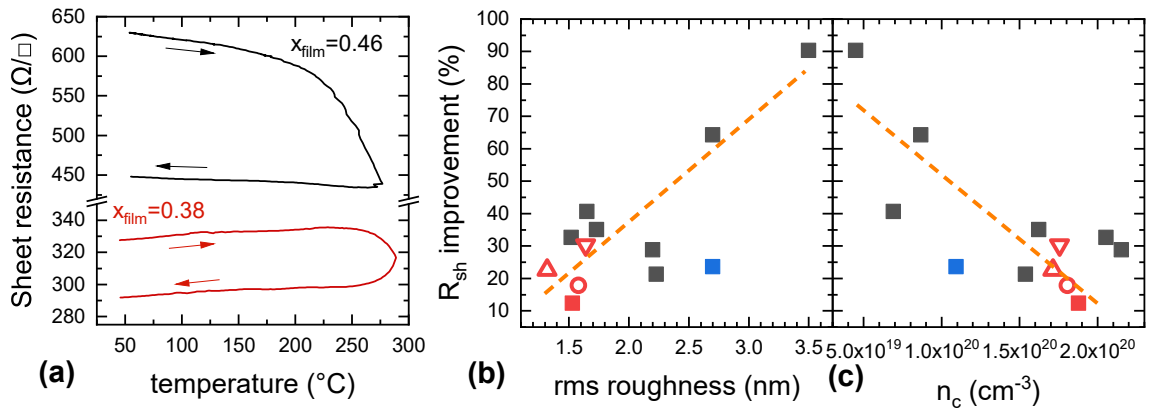

Figure 5: (a) Changes in the sheet resistance of SP grown a-ZTO samples during annealing in nitrogen atmosphere for two samples (x_{film}=0.38, x_{film}=0.46). Improvement of the sheet resistance during the anneal cycle as a function of the samples rms roughness (b) and carrier concentration n_c (c).

the dominant mechanism ($1/\mu = 1/\mu_{gb} + 1/\mu_{ii}$). In related crystalline material, such as ZnO, GB scattering plays a major role in the transport, specifically in films with lower carrier concentration and if the sample has been exposed to oxygen at elevated temperature. The latter leads to a large number of trap states at the interface between grains, accompanied with a depletion layer within the grain which becomes wider the lower the carrier concentration.[37,39–41] We suspect a similar mechanism to be responsible for the SP grown a-ZTO.

Figure 5 shows the resistance change of two samples with x_{film}=0.38 and x_{film}=0.46 when they are heated to 290°C in a full nitrogen atmosphere. This annealing temperature has been chosen to be significantly below the nominal growth temperature in order to avoid potential recrystallisation of the otherwise amorphous material. Similar to ZnO the sample resistivity is reduced irreversibly once heated above 250°C, consistent with the exchange of oxygen species at the grain interface by passivating N_2 molecules. Once cooled the improvement in conductivity remains, leaving the GB passivated. As with ZnO the improvement is larger for samples with lower carrier concentration, indicating the same mechanism.[37] The improvement also scales with the rms roughness, showing that more granular films with a higher surface area are more dramatically changed by the annealing.

Independent of the discussed changes in stoichiometry and morphology, all samples remain highly transparent. UV-VIS transmittance and reflectance spectra, as well as the absorption co-

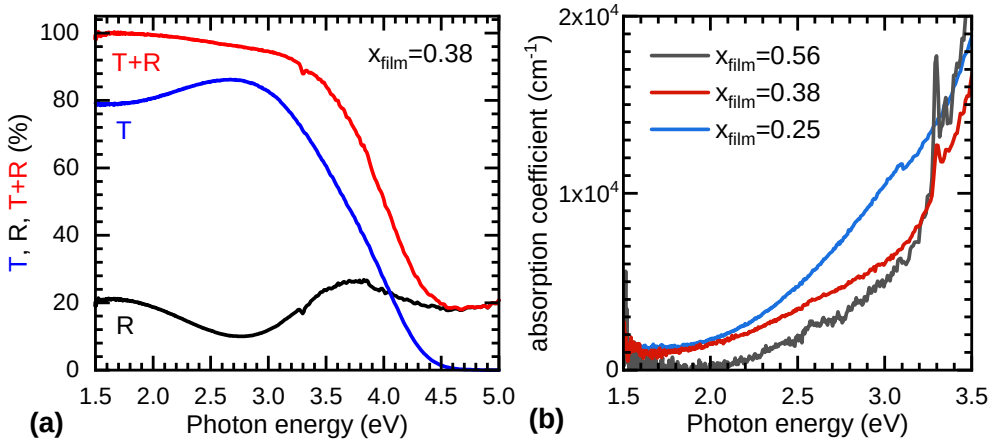

Figure 6: (a) Transmittance and reflectance spectra of a 60nm thick film (x_{film}=0.38). (b) absorption coefficient for samples with varying x_{film}.

efficient calculated from T, R, and the known film thickness are displayed in Figure 6. A high transmittance in the entire range with a film related absorption tail, specifically for Sn-rich samples, is observed. The band gap of the films is above the glass substrate absorption edge and can not be measured here. The increased absorption in Sn-rich samples has been previously seen in a-ZTO films grown by other methods.[35]

We believe the above demonstrates the key role that chamber geometry plays in the optimisation of a-ZTO. We highlight that the film morphology in SP grown films strongly depends on film growth rates and solution nebulisation, which in themselves depend on used molarity, chamber geometry and the type of nozzle. Smoother films are typically observed at reduced molarity, smaller droplet size, and narrow droplet distribution. In the case of a-ZTO the additional challenge created by the kinetic limitation of the Sn precursor results in a substantial change in a growth rate depending on x_{sol}, which has a knock on effect on the defect formation within the film. For instance, observed higher carrier concentrations in the Sn rich regime, which show higher growth rates, but may compromise the morphology, and hence carrier mobility, by creating rougher, more granular films. For this specific growth setup we therefore see an optimum conductivity for samples balancing these two opposing trends. For other instruments, while the same chemical and kinetic limitations are expected, the point for the optimum solution composition may vary. Understanding

and accounting for the role of system limitations will thus be essential in optimising and enhancing a performance of spray grown a-ZTO.

4 Conclusions

In summary, we demonstrated a successful growth of low roughness a-ZTO exhibiting a record-breaking electrical performance amid films deposited by inexpensive chemical synthesis methods. Careful control of deposition parameters is needed to tune composition and their electrical properties which is important for many applications. The resistivity values are found to be highly competitive with PVD deposited samples despite the constraints arising from the specifics of the utilised deposition system. We expect that more specialised system with a superior nebuliser could help overcome these limitations to push conductivity of a-ZTO even higher. Despite the granular nature of the films, carrier mobilities of $\approx$10 cm^2/Vs are acheieved. This bodes well for the prospect of using a-ZTO in ink-jet printed films from a nanoparticle (NP) suspension. In that case even room temperature deposition may be feasible as the NP synthesis could be decoupled from the film deposition. Our results on granular amorphous samples grown by SP show that, while there is a limitation in the transport, it is not as excessive as seen in other crystalline TCOs.

5 Acknowledgements

This work was supported by Science Foundation Ireland [grant number 12/IA/1264], Irish Research Council Laureate Award [grant number IRCLA/2019/171]. A.Z. and K.Z. would like to thank the Government of Republic of Kazakhstan under the Bolashak program for a PhD funding.

References

(1) Kamiya, T.; Nomura, K.; Hosono, H. Present Status of Amorphous In–Ga–Zn–O Thin-Film Transistors. *Science and Technology of Advanced Materials* **2010**, *11*, 044305.

(2) Nomura, K.; Ohta, H.; Takagi, A.; Kamiya, T.; Hirano, M.; Hosono, H. Room-Temperature Fabrication of Transparent Flexible Thin-Film Transistors using Amorphous Oxide Semiconductors. *Nature* **2004**, *432*, 488–492.

(3) Bomhard, E. M. The Toxicology of Indium Oxide. *Environmental Toxicology and Pharmacology* **2018**, *58*, 250–258.

(4) Nakamura, E.; Sato, K. Managing the Scarcity of Chemical Elements. *Nature Materials* **2011**, *10*, 158–161.

(5) Molkenova, A.; Khamkhash, L.; Zhussupbekova, A.; Zhussupbekov, K.; Sarsenov, S.; Taniguchi, I.; Shvets, I. V.; Atabaev, T. S. Solution-Based Deposition of Transparent Eu-Doped Titanium Oxide Thin Films for Potential Security Labeling and UV Screening. *Nanomaterials* **2020**, *10*, 1132.

(6) Norton, E.; Farrell, L.; Zhussupbekova, A.; Mullarkey, D.; Caffrey, D.; Papanastasiou, D. T.; Oser, D.; Bellet, D.; Shvets, I. V.; Fleischer, K. Bending Stability of Cu0.4CrO2—A Transparent P-type Conducting Oxide for Large Area Flexible Electronics. *AIP Advances* **2018**, *8*, 085013.

(7) Morales-Masis, M.; Wolf, S. D.; Woods-Robinson, R.; Ager, J. W.; Ballif, C. Transparent Electrodes for Efficient Optoelectronics. *Advanced Electronic Materials* **2017**, *3*, 1600529.

(8) Husein, S.; Medvedeva, J. E.; Perkins, J. D.; Bertoni, M. I. The Role of Cation Coordination in the Electrical and Optical Properties of Amorphous Transparent Conducting Oxides. *Chemistry of Materials* **2020**, *32*, 6444–6455.

(9) Medvedeva, J. E.; Buchholz, D. B.; Chang, R. P. H. Recent Advances in Understanding the Structure and Properties of Amorphous Oxide Semiconductors. *Advanced Electronic Materials* **2017**, *3*, 1700082.

(10) Lorenz, M. et al. The 2016 oxide electronic materials and oxide interfaces roadmap. *Journal of Physics D: Applied Physics* **2016**, *49*, 433001.

(11) Chiang, H. Q.; Wager, J. F.; Hoffman, R. L.; Jeong, J.; Keszler, D. A. High Mobility Transparent Thin-Film Transistors with Amorphous Zinc Tin Oxide Channel Layer. *Appl. Phys. Lett.* **2005**, *86*, 013503.

(12) Rucavado, E.; Jeangros, Q.; Urban, D. F.; Holovský, J.; Remes, Z.; Duchamp, M.; Landucci, F.; Dunin-Borkowski, R. E.; Körner, W.; Elsässer, C.; Hessler-Wyser, A.; Morales-Masis, M.; Ballif, C. Enhancing the Optoelectronic Properties of Amorphous Zinc Tin Oxide by Subgap Defect Passivation: A Theoretical and Experimental Demonstration. *Phys. Rev. B 95*, 245204.

(13) Morales-Masis, M.; Dauzou, F.; Jeangros, Q.; Dabirian, A.; Lifka, H.; Gierth, R.; Ruske, M.; Moet, D.; Hessler-Wyser, A.; Ballif, C. An Indium-Free Anode for Large-Area Flexible OLEDs: Defect-Free Transparent Conductive Zinc Tin Oxide. *Advanced Functional Materials* **2016**, *26*, 384–392.

(14) Rucavado, E.; Graužinytė, M.; Flores-Livas, J. A.; Jeangros, Q.; Landucci, F.; Lee, Y.; Koida, T.; Goedecker, S.; Hessler-Wyser, A.; Ballif, C.; Morales-Masis, M. New Route for "Cold-Passivation" of Defects in Tin-Based Oxides. *The Journal of Physical Chemistry C* **2018**, *122*, 17612–17620.

(15) Hosono, H.; Yasukawa, M.; Kawazoe, H. Novel Oxide Amorphous Semiconductors: Transparent Conducting Amorphous Oxides. *Journal of Non-Crystalline Solids* **1996**, *203*, 334–344.

(16) Chandra, R. D.; Rao, M.; Zhang, K.; Prabhakar, R. R.; Shi, C.; Zhang, J.; Mhaisalkar, S. G.; Mathews, N. Tuning Electrical Properties in Amorphous Zinc Tin Oxide Thin Films for Solution Processed Electronics. *ACS Applied Materials & Interfaces* **2013**, *6*, 773–777.

(17) Jackson, W. B.; Hoffman, R. L.; Herman, G. S. High-Performance Flexible Zinc Tin Oxide Field-Effect Transistors. *Appl. Phys. Lett.* **2005**, *87*, 1–3.

(18) Fernandes, C.; Santa, A.; Santos, Â.; Bahubalindruni, P.; Deuermeier, J.; Martins, R.; Fortunato, E.; Barquinha, P. A Sustainable Approach to Flexible Electronics with Zinc-Tin Oxide Thin-Film Transistors. *Advanced Electronic Materials* **2018**, *4*, 1800032.

(19) Pandey, R.; Wie, C. H.; Lin, X.; Lim, J. W.; Kim, K. K.; Hwang, D. K.; Choi, W. K. Fluorine Doped Zinc Tin Oxide Multilayer Transparent Conducting Oxides for Organic Photovoltaic Cells. *Solar Energy Materials and Solar Cells* **2015**, *134*, 5–14.

(20) Dutta, S.; Dodabalapur, A. Zinc Tin Oxide Thin Film Transistor Sensor. *Sensors and Actuators B: Chemical* **2009**, *143*, 50–55.

(21) Dang, G. T.; Kawaharamura, T.; Furuta, M.; Allen, M. W. Zinc Tin Oxide Metal Semiconductor Field Effect Transistors and their Improvement under Negative Bias (illumination) temperature stress. *Appl. Phys. Lett.* **2017**, *110*, 073502.

(22) Schlupp, P.; Vogt, S.; von Wenckstern, H.; Grundmann, M. Low voltage, high gain inverters based on amorphous zinc tin oxide on flexible substrates. *APL Materials* **2020**, *8*, 061112.

(23) Rajachidambaram, J. S.; Sanghavi, S.; Nachimuthu, P.; Shutthanandan, V.; Varga, T.; Flynn, B.; Thevuthasan, S.; Herman, G. S. Characterization of Amorphous Zinc Tin Oxide Semiconductors. *J. Mater. Res.* **2012**, *27*, 2309–2317.

(24) Zhussupbekova, A.; Kaisha, A.; Vijayaraghavan, R. K.; Fleischer, K.; Shvets, I. V.; Caffrey, D. Importance of Local Bond Order to Conduction in Amorphous, Transparent, Conducting Oxides: The Case of Amorphous ZnSnOy. *ACS Appl. Mater. Interfaces* **2019**, *11*, 44399–44405.

(25) Jayaraj, M. K.; Saji, K. J.; Nomura, K.; Kamiya, T.; Hosono, H. Optical and Electrical Properties of Amorphous Zinc Tin Oxide Thin Films Examined for Thin Film Transistor

Application. *Journal of Vacuum Science & Technology B: Microelectronics and Nanometer Structures* **2008**, *26*, 495.

(26) Park, J.; Oh, K.-T.; Kim, D.-H.; Jeong, H.-J.; Park, Y. C.; Kim, H.-S.; Park, J.-S. High-Performance Zinc Tin Oxide Semiconductor Grown by Atmospheric-Pressure Mist-CVD and the Associated Thin-Film Transistor Properties. *ACS Appl. Mater. Interfaces* **2017**, *9*, 20656–20663.

(27) Chang, Y.-J.; Lee, D.-H.; Herman, G. S.; Chang, C.-H. High-Performance, Spin-Coated Zinc Tin Oxide Thin-Film Transistors. *Electrochemical and Solid-State Letters* **2007**, *10*, H135.

(28) Kim, Y. J.; Oh, S.; Yang, B. S.; Han, S. J.; Lee, H. W.; Kim, H. J.; Jeong, J. K.; Hwang, C. S.; Kim, H. J. Impact of the Cation Composition on the Electrical Performance of Solution-Processed Zinc Tin Oxide Thin-Film Transistors. *ACS Appl. Mater. Interfaces* **2014**, *6*, 14026–14036.

(29) Branquinho, R.; Salgueiro, D.; Santa, A.; Kiazadeh, A.; Barquinha, P.; Pereira, L.; Martins, R.; Fortunato, E. Towards Environmental Friendly Solution-Based ZTO/AlOx TFTs. *Semiconductor Science and Technology* **2015**, *30*, 024007.

(30) Sanctis, S.; Koslowski, N.; Hoffmann, R.; Guhl, C.; Erdem, E.; Weber, S.; Schneider, J. J. Toward an Understanding of Thin-Film Transistor Performance in Solution-Processed Amorphous Zinc Tin Oxide (ZTO) Thin Films. *ACS Applied Materials & Interfaces* **2017**, *9*, 21328–21337.

(31) Han, W.; Chang, K. Subgap States near the Conduction-Band Edge Due to Undercoordinated Cations in Amorphous In-Ga-Zn-O and Zn-Sn-O Semiconductors. *Physical Review Applied* **2016**, *6*, 044011.

(32) Caffrey, D.; Zhussupbekova, A.; Vijayaraghavan, R. K.; Ainabayev, A.; Kaisha, A.; Sugurbekova, G.; Shvets, I. V.; Fleischer, K. Crystallographic Characterisation of Ultra-Thin, or

Amorphous Transparent Conducting Oxides—The Case for Raman Spectroscopy. *Materials* **2020**, *13*, 267.

(33) Eifert, B.; Becker, M.; Reindl, C. T.; Giar, M.; Zheng, L.; Polity, A.; He, Y.; Heiliger, C.; Klar, P. J. Raman Studies of the Intermediate Tin-Oxide Phase. *Physical Review Materials* **2017**, *1*.

(34) Rovisco, A.; Branquinho, R.; Martins, J.; Oliveira, M. J.; Nunes, D.; Fortunato, E.; Martins, R.; Barquinha, P. Seed-Layer Free Zinc Tin Oxide Tailored Nanostructures for Nanoelectronic Applications: Effect of Chemical Parameters. *ACS Applied Nano Materials* **2018**, *1*, 3986–3997.

(35) Wahila, M. J.; Lebens-Higgins, Z. W.; Butler, K. T.; Fritsch, D.; Treharne, R. E.; Palgrave, R. G.; Woicik, J. C.; Morgan, B. J.; Walsh, A.; Piper, L. F. J. Accelerated Optimization of Transparent, Amorphous Zinc-Tin-Oxide Thin Films for Optoelectronic Applications. *APL Mater.* **2019**, *7*, 022509.

(36) Arca, E.; Fleischer, K.; Shvets, I. V. Influence of the Precursors and Chemical Composition of the Solution on the Properties of ZnO Thin Films Grown by Spray Pyrolysis. *The Journal of Physical Chemistry C* **2009**, *113*, 21074–21081.

(37) Ali, D.; Butt, M. Z.; Coughlan, C.; Caffrey, D.; Shvets, I. V.; Fleischer, K. Nitrogen Grain-Boundary Passivation of In-Doped ZnO Transparent Conducting Oxide. *Physical Review Materials* **2018**, *2*.

(38) Perednis, D.; Gauckler, L. J. Thin Film Deposition Using Spray Pyrolysis. *Journal of Electroceramics* **2005**, *14*, 103–111.

(39) Vai, A. T.; Kuznetsov, V. L.; Jain, H.; Slocombe, D.; Rashidi, N.; Pepper, M.; Edwards, P. P. The Transition to the Metallic State in Polycrystallinen-type Doped ZnO Thin Films. *Zeitschrift Für Anorganische und Agemeine Chemie* **2014**, *640*, 1054–1062.

(40) Ellmer, K. Resistivity of Polycrystalline Zinc Oxide Films: Current Status and Physical Limit. *Journal of Physics D: Applied Physics* **2001**, *34*, 3097–3108.

(41) Sato, Y.; Yamamoto, T.; Ikuhara, Y. Atomic Structures and Electrical Properties of ZnO Grain Boundaries. *Journal of the American Ceramic Society* **2007**, *90*, 337–357.

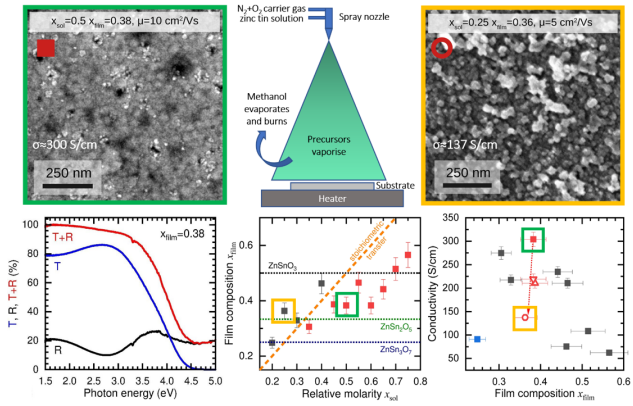

Figure 7: Abstract Graphic